Fast Detection and Removal of Glare in Gray Scale Laparoscopic Images

Nefeli Lamprinou and Emmanouil Z. Psarakis
Department of Computer Engineering & Informatics, University of Patras, Rion Patras, Greece

Keywords: Image Inpainting, Non-blind Inpainting.

Abstract: Images captured by laparoscopic cameras, often suffer from glare due to specular reflections from surgical tools and some tissue surfaces that can disturb the attention of surgeon. In this paper, inspired by their form, the photometric distortions caused by specular reflections are modeled as the superposition of a smooth and a pulse shaped curve. Based on this model a new fast technique for the detection and removal of glare in gray scale laparoscopic images is proposed. The proposed technique, as well as other state of the art image inpainting algorithms are used in a number of experiments based on artificial and real laparoscopic data, and the proposed algorithm seems to outperform its rivals.

1 INTRODUCTION

Glare is a source of major problems for automated image analysis systems, as it destroys all information in affected pixels, a fact that can introduce artifacts in feature's extraction algorithms. Image inpainting is the process of reconstructing lost or deteriorated regions in an image (Bertalmio et al., 2000). Many inpainting techniques have been applied in the field of the medical imaging in order to remove specular reflections.
Image inpainting methods can be broadly divided into the following two categories:

- non-blind inpainting and
- blind inpainting.

In the non-blind inpainting, the regions that need to be filled-in are provided to the algorithm a priori, whereas in blind inpainting, no information about the locations of the corrupted pixels is given and consequently the algorithm must additionally identify the pixels that require inpainting. The state-of-the-art non-blind inpainting algorithms can perform very well on removing text, doodle, or even very large objects (Bertalmio et al., 2000). Some image denoising methods, after modification, can also be applied to non-blind image inpainting with state-of-the-art results (Mairal et al., 2008).

Inpainting techniques tailored to repair the glare due to specular reflections in laparoscopic images follow. In (Lange, 2005) a feature based approach is used for the detection of the centers of regions that have been affected by the glare. In order to discover the total extent of glare's regions the use of morphological operators, adaptive thresholding techniques and the watershed transform is proposed. (Yang et al., 2010) use a bilateral filter, guided by the maximum diffuse chromaticity, as well as a technique for its fast estimation. In (Meslouhi et al., 2011) a method based on Dichromatic Reflection Model (Artusi et al., 2011) and multi-resolution (Ogden et al., 1985) inpainting techniques is presented. Two real time techniques based on the contrast weighting and intensity subtraction are proposed in (Xi and White, 2011). (Shabat and Averbuch, 2012) propose a matrix completion technique that uses as regularizers the nuclear or the spectral norm of the matrix. Finally, in (Marcinczak and Grigat, 2013) the limited accuracy that can be achieved by thresholding techniques is demonstrated and a hybrid scheme based on closed contours and thresholding is proposed.

Blind inpainting, however, is a much harder problem. Such a technique based on matrix completion technique using l_0 norm, is proposed in (Yan, 2013). (Queiroz and Ren, 2014) in order to identify the glare's regions propose a segmentation method based on sparse and low rank matrix decomposition techniques using robust PCA.

In this paper, inspired by their form, the photometric distortions caused by specular reflections are modeled as the superposition of a smooth and a pulse shaped curve. Based on this model a new fast technique for the detection and removal of glare in gray scale laparoscopic images is proposed.

Lamprinou, N. and Psarakis, E.
Fast Detection and Removal of Glare in Gray Scale Laparoscopic Images.
DOI: 10.5220/0006654202060212
In *Proceedings of the 13th International Joint Conference on Computer Vision, Imaging and Computer Graphics Theory and Applications (VISIGRAPP 2018) - Volume 4: VISAPP*, pages 206-212
ISBN: 978-989-758-290-5

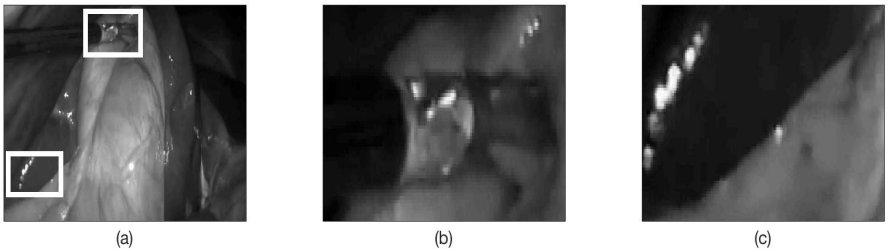

Figure 1: (a): Laparoscopic images with specular reflections due to (b): the surgical tool and (c): the biological tissue (please see text).

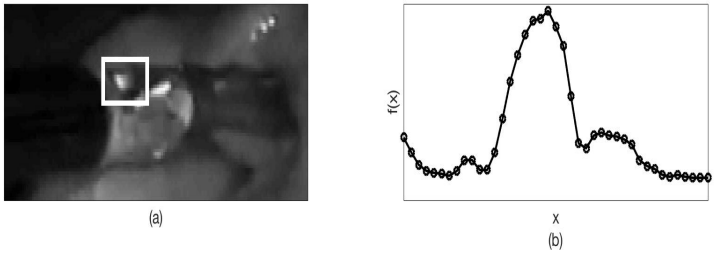

Figure 2: (a): Glare in a laparoscopic image due to the surgical tool. (b): A specific line of the squared region shown in (a).

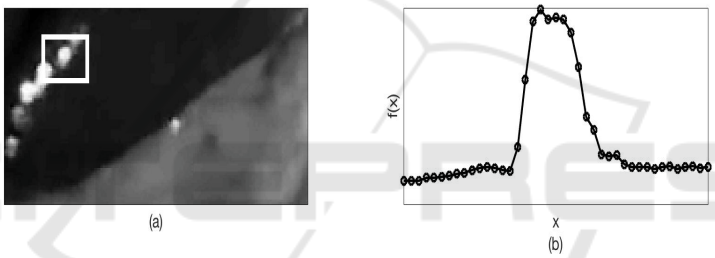

Figure 3: (a): Glare in a laparoscopic image due to the biological tissue. (b): A specific line of the squared region shown in (a).

2 SPECULAR REFLECTIONS AND GLARE

As it was already mentioned, specular reflections create strong photometric distortions in laparoscopic images. Their number, strength as well as shape, are strongly depended on biological surface angle, camera's light angle, viewing angle as well as the surgical tools when they are on the camera's field of view (see Figure 1). It is clear that all these photometrically distorted parts of laparoscopic images should be properly repaired in order to facilitate the tasks of the surgeon. To this end let us zoom into two lines of the glares shown in Figure 2 and 3 due to surgical tool and the biological tissue respectively. Based on these figures[1] we are going to adopt a simple model that can be used for the description for the aforementioned distortions.

Let $f(x)$ be an image line having K specular reflections of width $W_k = x_{k+1} - x_k,\ k = 0,1,\cdots,K-1$ each. Then, the following model for the image profile is considered:

$$f(x) = f_c(x) + \sum_{k=0}^{K-1} \alpha_k \big(u(x-x_k) - u(x-x_{k+1})\big) \quad (1)$$

where $f_c(x)$ the continuous component of the image, $\alpha_k,\ k = 0,1,\cdots,K-1$ the K positive heights of the specular reflections and $u(x)$ the step function.

By taking into account the following weak equality $u^{(1)}(x) = \delta(x)$ where $\delta(x)$ the distribution delta of Dirac, the following relation holds:

$$f^{(1)}(x) = f_c^{(1)}(x) + \sum_{k=0}^{K-1} \alpha_k \big(\delta(x-x_k) - \delta(x-x_{k+1})\big). \quad (2)$$

Having defined the specular reflections model, our goal now is to develop an appropriate technique to solve the associated estimation problem.

[1] It is clear that deconvolving the image line by an appropriate kernel which should be strongly related to the PSF of the gray scale laparoscopic camera, will make our proposition stronger.

Given the image line profile $f(x)$, let us consider that the points $x_k,\ k = 0,1,\cdots,K-1$ have been detected and thus they are known. Then, for each pair $(x_k,\ x_{k+1})$, of the aforementioned points, the following equations must hold:

$$\begin{aligned} f(x_k) &= f_c(x_k) + \alpha_k && (3)\\ f^{(1)}(x_k) &= f_c^{(1)}(x_k) + \alpha_k && (4)\\ f^{(1)}(x_k^-) &= f_c^{(1)}(x_k^-) && (5)\\ f(x_{k+1}) &= f_c(x_{k+1}) + \alpha_k && (6)\\ f^{(1)}(x_{k+1}) &= f_c^{(1)}(x_{k+1}) - \alpha_k && (7)\\ f^{(1)}(x_{k+1}^+) &= f_c^{(1)}(x_{k+1}^+), && (8) \end{aligned}$$

where $x^-,\ x^+$ denotes that we are approaching the point x from left and right respectively. It is clear that if the derivative of $f(x)$ is known and based on the continuity of its continuous counterpart it is an easy task to properly combine Eqs (3-8) to compute the desired unknown constant α_k. However, the aforementioned derivative is unknown and in addition only a sequence $f[n]$ resulting from the uniform sampling of the function $f(x)$ is known. Thus, it is necessary to reformulate the problem at hand in a more properly stated form where the sequence $f[n]$ instead of function $f(x)$ is considered to be known. To this end image's line model (Eq. (1)) as well as its derivative (Eq. (2)) are re-expressed into the following discrete form:

$$f[n] = f_c[n] + \sum_{k=0}^{K-1} \alpha_k \big(u[n-n_k] - u[n-n_{k+1}]\big) \quad (9)$$

$$d_f[n] = d_{f_c}[n] + \sum_{k=0}^{K-1} \alpha_k \big(\delta[n-n_k] - \delta[n-n_{k+1}]\big), \quad (10)$$

where $f[.],\ d_f[n]$ are the discrete counterparts of the functions $f(.),\ f^{(1)}(.)$ and $u[.],\ \delta[.]$ is the step and the kronecker sequence respectively.

Having defined the discrete counterparts of Eq. (1) and (2), in the next section we define the discrete counterparts of Eqs (3-8).

3 THE PROPOSED APPROACH

The discrete counterpart of Eqs (3) and (6) can be easily defined. However, the discrete counterparts of the remaining ones are not so straight forward defined. Note that all remaining equations are related to the derivative of the image line $f(x)$. The use of derivative-based filters in signal detection problems has been well documented in the relative literature. These filters have the ability to remove the non-stationary component of the signal, while at the same time preserve abrupt changes, which is highly desirable in problems of this nature. Note however that in the case of discrete time signals, there are three possible approximations of the signal derivative; namely the forward, the backward, and the forward-backward first-order difference operators. Although the third one is the most commonly used in signal detection problems, in this work we propose the use of the first two, i.e. the forward and the backward difference operator. Specifically, we propose the use of the *backward* difference operator, i.e:

$$d_{f^-}[n] = f[n] - f[n-1] \quad (11)$$

at the rising edge of the sequence, that is at the point n_k, and the use of the $forward$ difference operator, i.e.:

$$d_{f^+}[n] = f[n+1] - f[n] \quad (12)$$

at the falling one, that is at the point n_{k+1}.

We must stress at this point that our choice is in complete accordance with Eqs (5) and (8) respectively. Concluding, given the pair of points $n_k,\ n_{k+1}$ the following relations must hold:

$$\begin{aligned} d_{f^-}[n_k] &= d_{f_c^-}[n_k] + \alpha_k && (13)\\ d_{f^+}[n_{k+1}] &= d_{f_c^+}[n_{k+1}] - \alpha_k, && (14) \end{aligned}$$

where $d_{f_c^-}[.],\ d_{f_c^+}[.]$ [2] denote the backward and forward difference sequences of the sequence $f_c[.]$ respectively (a sequence, as it was already mentioned, resulting from the uniform sampling of continuous function $f_c(.)$). Note that Eqs (13-14) can be expressed in the form of the following underdetermined linear system:

$$M\mathbf{x}_{c_k} = \mathbf{b}_k \quad (15)$$

where

$$\begin{aligned} M &= \begin{bmatrix} 1 & 0 & 1 \\ 0 & 1 & -1 \end{bmatrix}\\ \mathbf{x}_{c_k} &= \begin{bmatrix} d_{f_c^-}[n_k] & d_{f_c^+}[n_{k+1}] & \alpha_k \end{bmatrix}^T\\ \mathbf{b}_k &= \begin{bmatrix} d_{f^-}[n_k] & d_{f^+}[n_{k+1}] \end{bmatrix}^T \end{aligned}$$

with the elements of vector $\mathbf{x}_{c_k}$ being the quantities that should be specified.

The above defined system is underdetermined, thus exhibiting an infinity of solutions, and the goal is to properly define the excess degrees of freedom. This can be achieved by using different cost functions for the specification of different optimum solutions in

[2] For space limitation reasons, from now on in some equations, the brackets from the forward and backward difference sequences will be omitted.

$\mathbb{R}^3$. For instance, the following constrained optimization problems can be defined:

$$(\mathcal{P}_l): \min_{\mathbf{x}_{c_k}\in\mathbb{R}^3} ||\mathbf{x}_{c_k}||_l \text{ subject to } M\mathbf{x}_{c_k} = \mathbf{b}_k,\ l = 0,1,2$$

and solved for the specification of candidate optimum solutions. In the next lemma the optimum solution of optimization problem $(\mathcal{P}_0)$ is specified.

Lemma 1: Consider the optimization problem $(\mathcal{P}_0)$. Then, its sparsest l_0 optimum solution is the following:

$$\mathbf{x}^{\star}_{c_k} = \begin{bmatrix} 0 \\ d_{f^-}[n_k] + d_{f^+}[n_{k+1}] \\ d_{f^-}[n_k] \end{bmatrix} \tag{16}$$

or

$$\mathbf{x}^{\star}_{c_k} = \begin{bmatrix} d_{f^-}[n_k] + d_{f^+}[n_{k+1}] \\ 0 \\ -d_{f^+}[n_{k+1}] \end{bmatrix}. \tag{17}$$

Both solutions are optimal and their l_0 norms are equal to 2.

Proof: The proof is easy and is omitted. □

In the next lemma the optimum solution of optimization problem $(\mathcal{P}_1)$ is specified. As we are going to see in this case the optimal solution is unique.

Lemma 2: Consider the optimization problem $(\mathcal{P}_1)$. Then, it attains its l_1 minimum value, i.e.:

$$||\mathbf{x}^{\star}_{c_k}||_1 = \begin{cases} |d_{f^-} + d_{f^+}| + d_{f^-}, & \text{if } d_{f^+} + d_{f^-} < 0 \\ \\ |d_{f^-} + d_{f^+}| - d_{f^+}, & \text{if } d_{f^+} + d_{f^-} > 0, \end{cases} \tag{18}$$

at:

$$\mathbf{x}^{\star}_{c_k} = \begin{cases} \begin{bmatrix} 0 \\ d_{f^-}[n_k] + d_{f^+}[n_{k+1}] \\ d_{f^-}[n_k] \end{bmatrix}, & \text{if } d_{f^+} + d_{f^-} < 0 \\ \\ \begin{bmatrix} d_{f^-}[n_k] + d_{f^+}[n_{k+1}] \\ 0 \\ -d_{f^+}[n_{k+1}] \end{bmatrix}, & \text{if } d_{f^+} + d_{f^-} > 0. \end{cases} \tag{19}$$

In addition, if $d_{f^+}[n_{k+1}] + d_{f^-}[n_k] = 0$, then, both solutions described from the branches of Eq. (19) are optimal.

Proof: The proof is easy and is omitted. □

Finally, the optimization problem $(\mathcal{P}_2)$ can be easily solved in the least squares sense thus finding the shortest candidate vector in the space $\mathbb{R}^3$. The optimum solution is given by the next lemma.

Lemma 3: Consider the constrained optimization problem $(\mathcal{P}_2)$. Then, it attains its l_2 minimum value:

$$||\mathbf{x}^{\star}_{c_k}||_2 = \sqrt{\frac{2}{3}(d^2_{f^-} + d^2_{f^+} + d_{f^-} d_{f^+})} \tag{20}$$

at:

$$\mathbf{x}^{\star}_{c_k} = \frac{1}{3}\begin{bmatrix} 2d_{f^-}[n_k] + d_{f^+}[n_{k+1}] \\ d_{f^-}[n_k] + 2d_{f^+}[n_{k+1}] \\ d_{f^-}[n_k] - d_{f^+}[n_{k+1}] \end{bmatrix} \tag{21}$$

Proof: The proof is easy and is omitted. □

We must stress at this point that since by definition $d_{f^-}[n_k]$, as the backward difference of the sequence defined in Eq. (11), is positive while $d_{f^+}[n_{k+1}]$, as its forward counterpart, is negative, all optimal solutions guaranty that the optimum value of α_k is positive, as it should be. However, the minimization of either the l_l, $l = 0,1,2$ norm does not seem to have any physical meaning. On the contrary, the l_l, $l = 0,1,2$ minimization of the related elements with the differences of the smooth counterpart of the sequence, is both attractive and has physical meaning.

To this end, let us define the following vectors:

$$\mathbf{x}_c(\alpha_k) = \left[d_{f_c^-}[n_k]\ d_{f_c^+}[n_{k+1}]\right]^T \tag{22}$$

$$\mathbf{i} = [-1\ 1]^T, \tag{23}$$

and rewrite the underdetermined system (15) as follows:

$$\mathbf{x}_c(\alpha_k) = \mathbf{b}_k + \alpha_k \mathbf{i} \tag{24}$$

where vector $\mathbf{x}_c(\alpha_k)$ is parameterized by glare's height α_k.

Our goal is now to specify the parameter α_k of the underdetermined system (24) by solving the following constrained optimization problems:

$$(\mathcal{P}_l'): \min_{\alpha_k\in\mathbb{R}} ||\mathbf{x}_c(\alpha_k)||_l \text{ s. to } \mathbf{x}_c(\alpha_k) = \mathbf{b}_k + \alpha_k\mathbf{i},\ l = 0,1,2.$$

It is evident that the optimum solutions of problems $(\mathcal{P}_l')$, $l = 0,1$ coincide with that of $(\mathcal{P}_l)$, $l = 0,1$. However, the solution of problem $(\mathcal{P}_2')$ does not coincide with the solution of $(\mathcal{P}_2)$. Specifically, the following lemma can be proved.

Lemma 4: The optimum solution of the constrained optimization problem $(\mathcal{P}_2)'$ is attained at:

$$\alpha^{\star}_k = \frac{d_{f^-}[n_k] - d_{f^+}[n_{k+1}]}{2}, \tag{25}$$

with

$$\mathbf{x}_c(\alpha_k)[1] = \mathbf{x}_c(\alpha_k)[2] = \frac{d_{f^-}[n_k] + d_{f^+}[n_{k+1}]}{2}. \tag{26}$$

This in turn, ensures the shortest Euclidean solution, that is:

$$||\mathbf{x}_c(\alpha^{\star}_k)||_2 = \frac{|d_{f^-}[n_k] + d_{f^+}[n_{k+1}]|}{\sqrt{2}}. \tag{27}$$

Proof: The proof is easy. From Eq. (20) the following relation holds:

$$||\mathbf{x}_c(\alpha_k)||^2_2 = 2\alpha^2_k + 2 < \mathbf{x}_k,\ \mathbf{i} > \alpha_k + ||\mathbf{x}_k||^2_2, \tag{28}$$

where $< \mathbf{y}, \mathbf{z} >$, $||\mathbf{y}||_2$ denotes the inner product of the vectors $\mathbf{y}$ and $\mathbf{z}$ and the euclidean length of the vector $\mathbf{y}$ respectively. The quadratic expressed by the right hand side of (25) achieves its minimum value for the value of α_k of (24).
This value is definitely positive since by definition $d_{f^-}[n_k]$ as the backward difference of the sequence defined in Eq. (11) is positive while $d_{f^+}[n_{k+1}]$ as its forward counterpart, is negative. Thus, the quantity defined by (24) is positive and this concludes the proof of the lemma. □

In the next section we evaluate the performance of the proposed technique.

4 EXPERIMENTAL RESULTS

In this section we are going to apply the proposed alignment technique by conducting a number of experiments. In addition, we will compare its performance in terms of the achieved alignment error, as well as its complexity against the methods proposed in (Shabat and Averbuch, 2012).

4.1 Artificially Distorted 1-D Signals

In this experiment we are going to apply the proposed technique on artificially distorted 1-D signals. In Figure 4.(c) such a distorted signal, resulting from the superposition of the smooth signal (see Fig. 4.(a)):

$$f_c[n] = cos(\frac{5\pi}{3}n^{\frac{1}{2}} + \frac{\pi}{8}n^{\frac{1}{3}})$$

and the specular glare (see Fig. 4.(b)):

$$s[n] = 17(u[n-100] - u[n-125])$$

respectively, is shown. In addition, its difference sequence $d_f[n]$ that can be used for the detection of glare's edges x_1, x_2, is shown in Figure 4.(d). The repaired signals obtained from the application of Lemma 2 and 4 respectively, are shown in Fig. 4.(e) and 4.(f) respectively. It is clear from this figure that the optimal solution of the optimization problem defined by Lemma 4 outperforms its rival resulting to a smoother reconstructed signal profile.

4.2 Real Laparoscopic Images

In this section we are going to apply the proposed technique in a large number of laparoscopic images and compare it against the techniques presented in (Shabat and Averbuch, 2012). Both approaches belong to the non-blind inpainting techniques thus requiring the support where the intensity of the image is known to be given as input. More specifically, they constitute varieties of matrix completion technique regularized by the nuclear and the spectral norm of the matrix respectively. For a given matrix A the aforementioned norms are defined as:

$$\begin{aligned} ||A||_\star &= \text{trace}\left(\sqrt{A^T A}\right) \\ ||A||_2 &= \max_{\mathbf{x}} \frac{||A\mathbf{x}||_2}{||\mathbf{x}||_2} = \sigma_{max}(A), \end{aligned}$$

where $\sigma_{max}(A)$ denotes the maximum singular value of matrix A.

To this end we apply the proposed technique as well as its rivals in 10K successive frames, each of size 360×640, of the cholecystectomy surgery video. The results we obtained from the application of the rivals to the specific image frame shown in Figure 5.(a) are shown in Figures 6, 7 and 8 respectively. From these figures, and in particular from the zoomed in figures, seems that the proposed technique outperforms its rivals since it results in smother, although not perfectly, repaired images.That was the case in all the experiments we have conducted. The mean complexity of the proposed algorithm is 2.2 secs and is error free in the glare free regions of the image. The mean complexity of its rivals, as well as the achieved MSE in the known regions of the frames, for different values of Tolerance for the completion matrix based techniques, are contained in Tables 1 and 2 respectively. From the contents of these tables, it is clear that the proposed technique outperforms its rivals. Finally we must stress at this point that the code of the spectral norm based completion matrix technique, uses *mex* file and this is the reason why it is faster than the nuclear norm based one.

Table 1: Performance of the Nuclear based Completion Matrix Technique.

Tolerance	10^{-1}	10^{-3}	10^{-5}	10^{-7}	10^{-9}
Time (sec)	2.52	2.12	5.60	13.77	40.12
Mean Error	10^{-1}	10^{-3}	10^{-5}	10^{-7}	0

Table 2: Performance of the Spectral based Completion Matrix Technique.

Tolerance	10^{-1}	10^{-3}	10^{-5}	10^{-7}	10^{-9}
Time (sec)	2.45	2.84	3.32	3.92	5.00
Mean Error	10^{-1}	0	0	0	0

5 CONCLUSIONS

The proposed technique was applied in a number of experiments and its superiority over other state of the

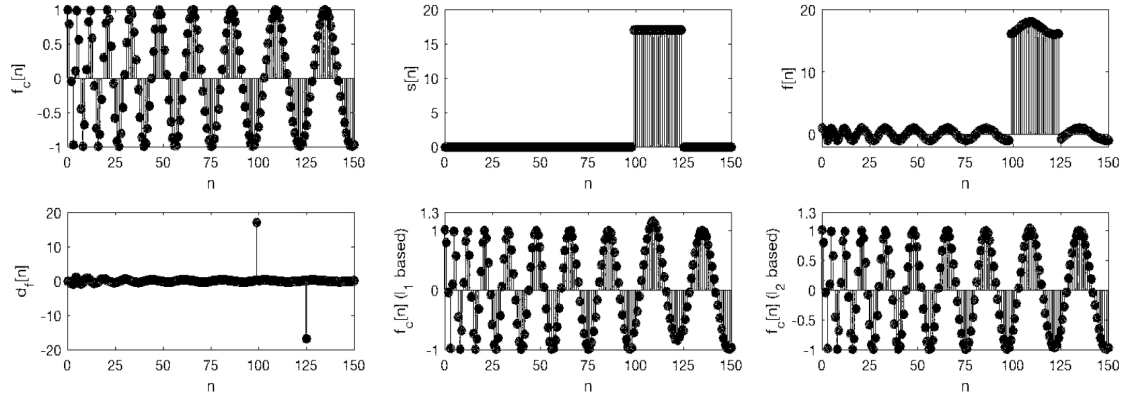

Figure 4: (c): An artificially distorted 1-D signal, resulting from the superposition of (a): the "smooth" signal, (b): the specular glare ($\alpha = 17$) and (d): its discrete difference sequence $d_f[n]$. The estimated "smooth" counterpart of signals, after the application of (f): Lemma 2 and (e): Lemma 4 on the contaminated signal (c).

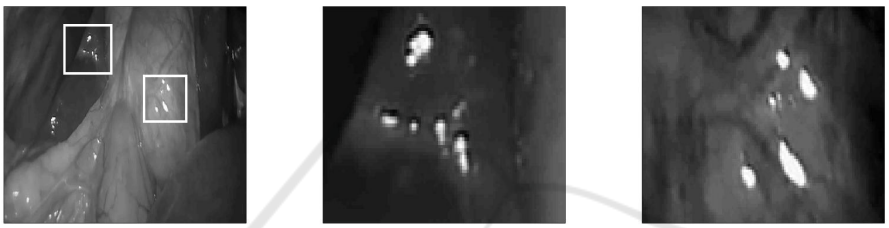

Figure 5: (a): An image extracted from a cholecystectomy surgery video containing photometric distortions due to specular reflections. (b), (c): Zoomed in of the squared regions shown in (a) with specular distortions in details.

Figure 6: The repaired image resulting from the application of the proposed technique on the specularly distorted image shown in Figure 5.(a). (b), (c): Zoomed in of the squared regions shown in (a) with specular distortions in details (please see text).

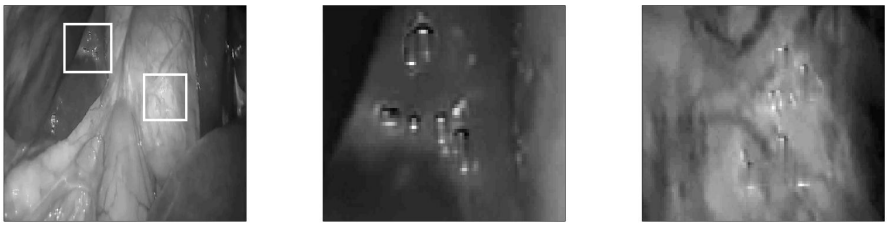

Figure 7: The repaired image resulting from the application of the Nuclear norm based Completion Matrix technique on the specularly distorted image shown in Figure 5.(a). (b), (c): Zoomed in of the squared regions shown in (a) with specular distortions in details (please see text).

art image alignment algorithms was indicated. However, the quality of the repaired images, even from the proposed method is not perfect, and this, as well as, its applicability to different kind of images is currently under investigation. This will make possible the comparison of the proposed technique against more re-

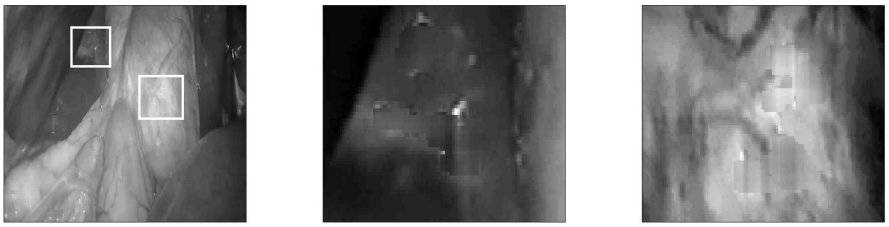

Figure 8: The repaired image resulting from the application of the Spectral norm based Completion Matrix technique on the specularly distorted image shown in Figure 5.(a). (b), (c): Zoomed in of the squared regions shown in (a) with specular distortions in details (please see text).

cent based on deep learning image inpainting methods. Moreover, in order to ensure the applicability of the proposed algorithm in real time video processing, the reduction of its mean complexity constitutes a vital issue that is also under investigation.

ACKNOWLEDGEMENTS

This research was supported by the State Scholarships Foundation (IKY) under contract 23384 – 2016 on behalf of the program "Research Projects for Excellence- IKY/Siemens".

REFERENCES

Artusi, A., Banterle, F., and Chetverikov, D. (2011). A survey of specularity removal methods. *Computer Graphics Forum*, 30(8):2208–2230.

Bertalmio, M., Sapiro, G., Caselles, V., and Ballester, C. (2000). Image inpainting. *Proceedings of the 27th Annual Conference on Computer Graphics and Interactive Techniques*, pages 417–424.

Lange, H. (2005). Automatic glare removal in reflectance imagery of the uterine cervix. In *Proceedings Medical Imaging*, volume 5747.

Mairal, J., Elad, M., and Sapiro, G. (2008). Sparse representation for color image restoration. *IEEE Transactions on Image Processing*, 17(1):53–69.

Marcinczak, J. M. and Grigat, R. R. (2013). Closed contour specular reflection segmentation in laparoscopic images. *International Journal of Biomedical Imaging, Hindawi Publishing Corporation*, 2013:1–6.

Meslouhi, O. E., Kardouchi, M., Allali, H., Gadi, T., and Benkaddour, Y. A. (2011). Automatic detection and inpainting of specular reflections for colposcopic images. *Central European Journal of Computer Science*, 1(3):341–354.

Ogden, J. M., Adelson, E. H., Bergen, J. R., and Burt, P. J. (1985). Pyramid-based computer graphics. *RCA Engineer*, 30(5):4–15.

Queiroz, F. and Ren, T. I. (2014). Automatic segmentation of specular reflections for endoscopic images based on sparse and low-rank decomposition. In *SIBGRAPI Conference on Graphics, Patterns and Images*.

Shabat, G. and Averbuch, A. (2012). Interest zone matrix approximation. *Electronic Journal of Linear Algebra*, 23(1):678–702.

Xi, E. A. W. and White, P. (2011). Methods for removing glare in digital endoscope images. *Surgical Endoscopy*, 25:3898–3905.

Yan, M. (2013). Restoration of images corrupted by impulse noise using blind inpainting and l_0 norm. *SIAM Journal of Imaging Sciences*, 6(3):1227–1245.

Yang, Q., Wang, S., and Ahuja, N. (2010). Real-time specular highlight removal using bilateral filtering. In *European Conference on Computer Vision (ECCV)*, pages 87–100.